1 **Photochemical aging of volatile organic compounds associated with oil and natural gas**

2 **extraction in the Uintah Basin, UT, during a wintertime ozone formation event**

3

4 **A. R. Koss[1,2], J. de Gouw[1,2], C. Warneke[1,2], J. B. Gilman[1,2], B. M. Lerner[1,2], M. Graus[1,2,*], B.**

5 **Yuan[1,2], P. Edwards[1,2,†], S. S. Brown[2], R. Wild[1,2], J. M. Roberts[2], T. S. Bates[3,4], P. K. Quinn[4]**

6

7 [1]{Cooperative Institute for Research in Environmental Sciences, Univ. of Colorado, Boulder,

8 CO, USA}

9 [2]{NOAA Earth System Research Laboratory, Chemical Sciences Division, Boulder, CO, USA}

10 [3]{Joint Institute for the Study of the Atmosphere and Ocean, University of Washington, Seattle,

11 WA}

12 [4]{NOAA/Pacific Marine Environmental Laboratory, Seattle, WA}

13 [*]{now at: Institute of Meteorology and Geophysics, Innsbruck University, Innsbruck, Austria}

14 [†]{now at: Department of Chemistry, University of York, York, YO10 5DD, UK}

15 Correspondence to: A. R. Koss (abigail.koss@noaa.gov)

16

17 **Abstract**

18 High concentrations of volatile organic compounds (VOCs) associated with oil and natural gas

19 extraction were measured during a strong temperature inversion in winter of 2013 at a rural site in

20 the Uintah Basin, Utah. During this period, photochemistry enhanced by the stagnant

21 meteorological conditions and concentrated VOCs led to high ozone mixing ratios (150ppbv). A

22 simple analysis of aromatic VOCs measured by proton-transfer-reaction mass-spectrometry (PTR-

23 MS) is used to estimate (1) VOC emission ratios (the ratio of two VOCs at the time of emission)

24 relative to benzene, (2) aromatic VOC emission rates, and (3) ambient OH radical concentrations.

25 These quantities are determined from a best fit to VOC:benzene ratios as a function of time. The

26 main findings are that (1) emission ratios are consistent with contributions from both oil and gas

27 producing wells; (2) the emission rate of methane ($27\text{-}57\text{x}10^3$ kg methane hr^{-1}), extrapolated from

28 the emission rate of benzene ($4.1\pm0.4\text{x}10^5$ molecules cm^{-3} s^{-1}), agrees with an independent estimate

29 of methane emissions from aircraft measurements in 2012; and (3) calculated daily OH

30 concentrations are low, peaking at $1\text{x}10^6$ molecules cm^{-3}, and are consistent with Master Chemical

31 Mechanism (MCM) modeling. The analysis is extended to photochemical production of

32 oxygenated VOCs measured by PTRMS and is able to explain daytime variability of these species.

33 It is not able to completely reproduce nighttime behavior, possibly due to surface deposition. Using

34 results from this analysis, the carbon mass of secondary compounds expected to have formed by

35 the sixth day of the stagnation event was calculated, then compared to the measured mass of

36 primary and secondary compounds. Only 17% of the expected secondary carbon mass is accounted

37 for by gas phase, aerosol, and snow organic carbon measurements. The disparity is likely due to

38 substantial amounts of unquantified oxygenated products.

39

40 **1. Introduction**

41 Natural gas, crude oil, and natural gas liquids are major fuel sources -- accounting for 54% of 2013

42 US domestic energy production -- and extraction of these resources has been rising substantially

43 since the mid 2000's (US Energy Information Administration, 2014). This activity is associated

44 with a range of possible environmental issues. Emissions due to extraction can: increase

45 atmospheric concentrations of methane, a greenhouse gas (Miller et al., 2013; Brandt et al., 2014);

46 directly impact local air quality through release of air toxics (Moore et al., 2014; Adgate et al.,

47 2014; Li et al., 2014); and contribute to photochemical ozone formation (Schnell et al., 2009;

48 Edwards et al., 2014; Carter and Seinfeld, 2012). Many scientific aspects of these processes are

49 uncertain. Emissions budgets of methane and other VOCs are poorly constrained and frequently

50 do not agree with inventory estimates (Brandt et al., 2014; Miller et al., 2013). Many variables can

51 affect the composition of emissions, including well life-cycle stage, extraction techniques, whether

52 the well is producing oil or gas, and diverse infrastructure/equipment components (Moore et al.,

53 2014; Litovitz et al., 2013; Allen et al., 2013). Wintertime ozone events, while sharing some

54 similarities with ozone formation typically seen in urban areas during the summer, occur in

55 different meteorological and chemical conditions and have attracted several recent measurement

56 and modeling investigations (Schnell et al., 2009; Kotamarthi and Holdridge, 2007; Carter and

57 Seinfeld, 2012; Edwards et al., 2013; Edwards et al., 2014).

58

59 The Uintah Basin, located in northeastern Utah, is a region of intense oil and natural gas extraction

60 activity. Approximately 4000 active oil-producing and 6500 gas-producing wells are located in a

61 10000 km^2 area, with an additional 1000 wells added each year (Utah Oil and Gas, 2014). In

62 January and February of 2012-2014, a suite of chemical and meteorological instrumentation was

63   deployed at Horse Pool, a remote site in the eastern part of the basin. Little active photochemistry

64   was observed in 2012, but in 2013 ground snow cover was accompanied by several sustained

65   periods of strong temperature inversion. Temperature inversions trap ozone precursors emitted by

66   oil and natural gas activity (VOCs and NO_x) and ozone close to the surface. Increased actinic flux

67   from reflective snow cover contributes to heightened ozone-producing photochemistry (Edwards,

68   2014). The gradual buildup of VOCs and ozone during a several day period of these conditions

69   can lead to very high mixing ratios – in this case, up to 5ppmC non-methane hydrocarbon and

70   150ppb ozone. VOCs are a fundamental component of the photochemistry that occurred during

71   these events, and so it is important to quantify (1) the rate at which VOCs are emitted from primary

72   sources ("emission rate"), (2) the source composition of the VOC mixture ("emission ratios"), and

73   (3) the degree of VOC oxidation.

74

75   In this paper, we analyze the photochemical aging of VOCs during an ozone formation period in

76   2013. We first examine primary, aromatic VOCs with a method that considers reaction with OH

77   and constant primary emission. This analysis provides information on the emission rate and

78   emission ratios of these VOCs, and the typical daily concentration of OH. We next investigate

79   oxygenated VOCs with a method that includes production and loss via OH chemistry and loss to

80   photolysis. This approach identifies oxygenated VOCs with substantial primary sources and

81   suggests rates of carbonyl formation from photochemistry. Finally, we calculate the organic carbon

82   mass balance of primary and product species. This defines overall VOC speciation and determines

83   the fraction of product species measured with the Horse Pool instrumentation.

84

85   **2. Methods**

86   **2. 1 Measurement site and instrumentation.**

87   The Horse Pool site is located in the central eastern part of the Uintah basin, approximately 30km

88   south of Vernal, Utah. Meteorological, gas, and particle-phase measurements were deployed

89   concurrently at the site from 15 Jan. - 29 Feb. 2012, 23 Jan. – 22 Feb. 2013, and 15 Jan. – 13 Feb.

90   2014. Data referenced in this paper are primarily from a proton-transfer-reaction mass-

91   spectrometer (PTR-MS), deployed in both 2012 and 2013, and a gas chromatograph with flame

92   ionization detection (GC-FID), deployed in 2013. Measurements from 2014 are not discussed in

93   this analysis.

94

95   PTR-MS uses chemical ionization with H_3O^+ ions to selectively detect VOCs (de Gouw and

96   Warneke, 2007). The technique is particularly sensitive to aromatic and small oxygenated VOCs,

97   but cannot detect small alkanes due to their low proton affinity. The instrument deployed at Horse

98   Pool uses a quadrupole mass filter with unit mass resolution that scans through a set of selected

99   ions every 38 seconds. Data are averaged to a 1-minute time scale. Calibrated measurement

100   accuracy is generally better than 20%, with a precision of 10%. The instrument is not able to

101   distinguish between isomers; e.g. a measurement of C8 aromatics comprises the sum of

102   ethylbenzene, o-, m-, and p- xylenes. Comparison with a high-resolution PTR- time-of-flight

103   spectrometer operated by the University of Wyoming (Warneke et al., 2015) indicates negligible

104   contribution from isobaric compounds (e.g., benzaldehyde).

105

106   The GC-FID deployed at Horse Pool resolves C2-C7 saturated and unsaturated hydrocarbons.

107   Ambient air passes through water and carbon dioxide traps, then into a liquid nitrogen cryogenic

108   VOC trap. VOCs are captured in the cryogenic trap for five minutes every half hour. After the

109   five-minute sampling period, compounds are injected onto a 50m Al_2O_3/KCl PLOT column and

110   analyzed using flame ionization detection. The accuracy and precision are dependent on compound

111   and sample flow rate, but are generally <20% and <5%, respectively. The instrument has been

112   previously described in more detail by Kuster *et al.* (2004).

113

114   Other measurements used in this paper include gas-chromatography mass-spectrometry (GC-MS)

115   operated in 2012 (Gilman et al., 2010), methane cavity ring-down spectroscopy (CaRDS, Picarro)

116   operated in 2013 (Crosson, 2008), organic aerosol via quartz filter collection/thermal desorption

117   in 2013 (Bates et al., 2004), snow organic carbon using a Shimadzu TOC-VCSH instrument in

118   2013, and organic peroxy nitrate (PAN) species by chemical ionization mass spectrometry (Slusher

119   et al., 2004). Some sulfur-containing species were measured (Li et al., 2014) but are not discussed

120   in this manuscript. Further details on sampling methods and conditions, meteorological

121   measurements, and calibrations are described in a summary report (Uinta Basin: 2013 Winter

122   Ozone   Study: Final   Report;   available   at

123   http://www.deq.utah.gov/locations/U/uintahbasin/ozone/strategies/studies/UBOS-2013.htm).

124

2.2 Data treatment

A stagnation event associated with high levels of ozone formation occurred from 29 Jan. to 10 Feb. 2013. A subset of this period, 31 Jan. 2013 20:48 (LT) through 08 Feb. 2013 05:29, is analyzed here (Fig. 1). This period captures the majority of the ozone formation event, is characterized by a strong temperature inversion, and avoids periods of higher wind on 31 Jan. and 08 Feb. Selecting these meteorological conditions minimizes changes in VOC concentrations and ratios due to mixing into or out of the basin.

Primary hydrocarbons and oxygenated compounds investigated are listed in Table 1. The majority of analysis was applied to compounds measured by PTR-MS. The fast time resolution of this instrument (1 minute) allows the separation of plumes of VOCs from nearby sources from the more regionally widespread, accumulated emissions in the basin. Additionally, restricting analyzed compounds to a single instrument helps eliminate instrumental variation. Additional compounds from the GC-FID data set were used to investigate the balance of primary and secondary species.

Concentrations of VOCs during an inversion event displayed rapid, diurnal, and multi-day variability (Fig. 2). Some of this variability is attributable to meteorology (such as changes in boundary layer height during the day, or temporary shifts in wind direction bringing pollution from nearby sources), and some to chemistry, but the relative contributions can be difficult to separate. Analysis of ratios of VOCs provides a way to isolate the effects of chemistry from meteorology. This is a common and flexible approach: applications have included determining the photochemical age of urban emissions (Roberts et al., 1984; de Gouw et al., 2005), quantifying halogen chemistry in arctic air (Jobson et al., 1994), and identifying contributions from oil and natural gas operations to ambient pollution (Gilman et al., 2013).

Measurements of primary compounds by PTR-MS showed frequent 1-3 minute duration episodes with very high mixing ratios, at least 50% higher than short-term average concentration. These spikes signify interception of plumes of un-aged emissions and are not representative of the bulk air composition at the Horse Pool site. An hourly running median was applied to separate longer-term variability from transitory primary emissions (Fig. 2). For consistency, an hourly running

156 median was also applied to oxygenated compounds. The ratio of each VOC to benzene was then

157 determined. Benzene is a well-calibrated compound with few interferences on the PTR-MS;

158 additionally, good agreement with other instrumentation (GC-FID and PTR-ToF) at the site affords

159 a high level of confidence in this measurement (Warneke et al., 2015).

160

161 **3. Results and Discussion**

162 **3.1 Primary compounds**

163 Primary compounds are defined as those species that are directly emitted and not formed by

164 photochemistry. The rate of change with time of a single, primary VOC can be written as

$$165 \quad \frac{d[VOC]}{dt} = P_{VOC} - k_{VOC}[OH][VOC] - \sum D_i[VOC] \tag{1}$$

166 where P_{VOC} is the emission rate of the VOC and k_{VOC} is the rate constant for the reaction of the

167 VOC with OH. P_{VOC} is a volumetric input with units of molecule cm^{-3} s^{-1} and describes how direct

168 emission increases observed VOC concentrations. The only chemical loss term included is reaction

169 with OH, the major oxidizing radical in this environment. Previous modeling has suggested that

170 VOC reactions with other radicals, such as $Cl^{\bullet}$, were negligible in comparison to reaction with OH

171 (Edwards et al., 2014). Additionally, reaction rates of the primary species considered here (C6-

172 C10 aromatics) with O_3 and NO_3 are at least several orders of magnitude lower than reaction rates

173 with OH (Atkinson and Arey, 2003). D_i are rate constants for first-order loss processes; e.g.

174 deposition, dilution, photolysis, etc. If two VOCs, "A" and "B", behave according to Equation (1),

175 we can derive the rate of change of their ratio ([A]/[B]) as follows:

$$176 \quad ratio(t) = \frac{[A](t)}{[B](t)} \tag{2a}$$

177 Using the partial derivatives of *ratio(t)* with respect to [A] and [B], the rate of change of the ratio

178 is:

$$179 \quad \frac{d(ratio)}{dt} = \frac{1}{[B]}\frac{d[A]}{dt} - \frac{[A]}{[B]^2}\frac{d[B]}{dt} \tag{2b}$$

180 Then, substituting Equation (1) for dA/dt and dB/dt, we arrive at:

$$181 \quad \frac{d(ratio)}{dt} = \frac{P_B}{[B]}(ER - ratio) + (ratio)[OH](k_B - k_A) + \sum(ratio)(D_{iB} - D_{iA}) \tag{2c}$$

182

183 The primary emission rate (P_B), emission ratio (ER), and the concentration of OH are unknown.

184 The emission ratio ($ER=P_A/P_B$) is the ratio of two VOCs in fresh emissions (time t = 0) and is a

185   measure of source composition. We consistently used benzene as the denominator in the ratio, so

186   that [B] = [benzene], P_B is the emission rate of benzene, *ER* is the emission ratio of a VOC to

187   benzene, and so on. Meteorological data and the measured ambient mixing ratio of benzene were

188   used to determine the number density of benzene ([B]) as a function of time. These values were

189   referenced directly when applying Equation (2c).

190

191   C6-C10 aromatic VOCs were selected for analysis of primary compounds because they have

192   readily identifiable parent masses, they are sensitively detected by PTR-MS, and have a relatively

193   wide range of reactivity with OH ($k_{OH} = 1.22 \times 10^{-12}\,s^{-1}$ to $56 \times 10^{-12}\,s^{-1}$). Application of this analysis

194   to VOCs measured by PTR-MS using Equation (2c) includes the following assumptions.

195

196   (1) For each first-order loss process, rate constants are nearly identical for aromatic compounds

197   ($D_{iA} = D_{iB} = D_i$). These loss processes include mixing out of the basin, photolysis, and deposition.

198   Mixing is dependent on dynamics and not on chemical characteristics, so mixing loss rate constants

199   should be identical for all VOCs with the same vertical concentration profile ($D_{mixing,B} -$

200    $D_{mixing,A} = 0$). We saw no evidence of differences in vertical gradients of aromatic species at

201   Horse Pool. As concentrations of VOCs in the background atmosphere were considerably smaller

202   than VOC concentrations inside the basin, changes in VOC ratios due to mixing in of background

203   air are negligible. Integrated UV absorption cross-sections of C6-C10 aromatic hydrocarbons are

204   small and similar to one another (Etzkorn et al., 1999), so $\left(D_{photolysis,B} - D_{photolysis,A}\right)$ is likely

205   negligible compared to primary emission and reaction with OH. The same argument can be made

206   for wet or dry deposition ($D_{deposition,B} - D_{deposition,A} \cong 0$), as monocyclic aromatic compounds

207   are structurally similar and have small solubilities in water. The terms ($D_{iB} - D_{iA}$) can therefore

208   be eliminated.

209

210   (2) Primary VOC emission rate and emission ratios are constant in time and similar in composition

211   across the basin – we cannot confidently parameterize a more complicated emissions scenario with

212   available data, nor is there any evidence supporting or reason to assume a change in emissions

213   with time of day.

214

215 (3) Finally, on an hourly scale, we assume that compounds are well mixed. The latter assumptions

216 are supported by aircraft measurements in Jan-Feb. 2013, which found elevated VOC

217 concentrations with similar ratios in all parts of the basin, including regions with varying intensities

218 and types of fossil fuel extraction activity (Oltmans et al., 2014). The time period analyzed,

219 characterized by a strong temperature inversion and light winds (Fig. 1), was specifically selected

220 to support these assumptions.

221

222 **3.1.1 Emission rates and ratios**

223 The analysis is first applied to night-time data only (any points where solar radiation is zero), to

224 estimate P_B and ER. During the night, OH is close to zero and Eq. (2c) reduces to

225 $$\frac{d(ratio)}{dt} = \frac{P_B}{[B]}(ER - ratio) \qquad (3)$$

226 This method, using only night-time data, reduces the number of free variables. It completely

227 separates primary emission from OH chemistry. Additionally, it allows the use of C9 and C10

228 aromatics measurements, as the OH rate constants for these groups are not well constrained.

229

230 The measured ratios of C7, C8, C9, and C10 aromatics to benzene were described using a best fit

231 of Eq. (3) to the data. The free parameters in this fit are P_B and ER. A best fit was determined

232 separately for each of the four aromatic ratios, providing four, similar, independent estimates of

233 P_B (Fig. 3) and four emission ratios to benzene (Table 2). We evaluate the fit by comparing

234 emission ratios to literature values and the composition of plumes from nearby sources, and,

235 second, by comparing emission rate to an independent estimate.

236

237 The derived emission ratios from this analysis represent an averaged source composition of all

238 point sources contributing VOCs to well-mixed air. In Fig. 4, the derived emission ratios are

239 compared to three other measurements of source composition in the Uintah basin: (1) Mobile

240 laboratory measurements taken at individual wellpads in 2012 (Warneke et al., 2014); (2) ambient

241 measurements taken at Horsepool in 2012 (Warneke et al., 2014); and (3) 2013 VOC enhancement

242 ratios in spikes above a 1-hour running median (discussed above). These spikes are likely plumes

243 of fresh emissions from nearby wellpads. The fastest-reacting C10 aromatic (1,2,4-

244 trimethylbenzene) had a peak daytime chemical lifetime against OH of about 30min. Seven other

245 wellpads were within 500m of the Horsepool site; given average wind speed (1.6m s^{-1}), this

246 corresponds to a 5 minute transport time – much shorter than the chemical lifetime of any of the
247 analyzed aromatic species. All three measurements are separated into gas-producing and oil-
248 producing well contributions; in mobile lab data, by type of wellpad sampled; in Horsepool data,
249 by correlation with wind direction (Warneke et al., 2014).

251 There is a clear distinction between oil and gas sources. The difference grows with carbon number;
252 i.e. gas producing-wells emit a lighter mixture of VOCs. Emission ratios suggested by our analysis
253 suggest significant contribution from both oil and gas sources. In addition to the oil/gas distinction,
254 there is a large range of variability in source composition of aromatic species. This variability is
255 difficult to represent in bulk emissions estimates and models. Together with supporting evidence
256 from aircraft that emissions were reasonably well mixed across the basin (Oltmans et al., 2014),
257 our analysis provides an independent measure of average emissions composition.

259 The average benzene emission rate was $4.1\pm0.4\text{x}10^5$ molecules cm^{-3} s^{-1}. To evaluate this emission
260 rate estimate, we compare to basin-wide methane emission measurements conducted by aircraft in
261 2012 (Karion et al., 2013). To our knowledge this is the only recent top-down emissions estimate
262 for the Uintah Basin. Karion et al. determined that basin-wide methane emissions were $55\pm15 \times$
263 10^3 kg hr^{-1}. To compare a volume-normalized estimate (molecules benzene cm^{-3} s^{-1}) to the whole-
264 basin estimate (kg methane hr^{-1}), we need (1) the emission ratio of methane to benzene and (2) the
265 total volume of the polluted layer during the 2013 ozone episode.

267 A strong correlation between methane and benzene is apparent from ground site measurements at
268 Horse Pool in 2012 and 2013 (Fig. 5). Aircraft flask samples taken in 2013 suggest that the
269 methane:benzene ratio is independent of location in the basin – it was similar in both the eastern
270 gas field and western oil field (Oltmans et al., 2014). The methane:benzene emission ratio was
271 approximated from 2012 measurements and 2013 plumes (ER=1330±80 ppbv/ppbv).

273 The polluted volume of the basin was determined from frequent ozonesonde measurements at a
274 number of locations in the basin, as well as aircraft profiles. They showed well mixed ozone
275 concentrations up 1600-1700 meters above sea level (100-200 meter above ground level at
276 Horsepool), above which mixing ratios decreased sharply (Oltmans et al., 2014). Taking the terrain

277   of the basin into account, we then integrate the volume of the basin from the surface to the mixing

278   height. The uncertainty in the basin wide methane emission estimate is dominated by the

279   uncertainty in this volume, and we report the values determined from minimum and maximum

280   polluted layer altitude (1600m – 1700m).

281

282   Using the methane:benzene ratio and the mixing volume of the basin, we derive an emission rate

283   of $(14\text{-}39)\times10^3$ kg methane hr^{-1}. This is lower than the Karion et al. estimate, but of the same

284   magnitude. An inspection of well locations in the basin shows that a significant fraction (40-50%)

285   of wells lie outside the polluted layer (Fig. 6). An aircraft flux measurement would have likely

286   included contributions from these wells, whereas our analysis only included wells emitting inside

287   the isolated polluted volume. A linear extrapolation based on the number of wells inside and

288   outside the polluted volume suggests an emission rate of $(27\text{-}57)\text{x}10^3$ kg methane hr^{-1}, which

289   overlaps with the Karion et al. value. Although this estimate is considerably less precise than the

290   aircraft flux measurement, it does confirm that the best-fit values of benzene emission rate are

291   plausible.

3.1.2 Concentration of OH radical

293   The full time series (both day and night) was analyzed over the buildup period, using Eq. (2c). The

294   primary emission term (P_B) and the emission ratio were fixed as determined from the night best

295   fits. The only remaining free variable is the concentration of OH.

296

297   The calculation requires OH rate constant (k_{OH}) for the aromatics. Measurements of C8 aromatics

298   in 2013 were not isomerically resolved by PTR-MS and represent the sum of ethylbenzene and *o-*

299   , *m-*, and *p*-xylenes. Speciated measurements of C8 aromatics by GC-MS were made in 2012,

300   when photochemical aging of VOCs was less active and the bulk air composition more closely

301   resembled primary emissions. The 2012 GC-MS measurements were used to compute a weighted

302   average OH rate constant for the C8 aromatics group. The OH rate constants for individual species

303   in this group are within a factor of 2.1 of the mean. The groups C9 and C10 aromatics contain a

304   much larger number of isomers, with a wider variance in OH rate constants. Not all these isomers

305   were measured by GC-MS in 2012, and some of the OH rate constants are unknown. Therefore,

306   the group average rate constant could not be constrained in the same way.

307

308   To parameterize the diurnal variation in OH, we constrained OH to be proportional to solar actinic

309   flux. It is well established that [OH] is strongly linearly correlated with UV light intensity (Hard

310   et al., 1986; Rohrer and Berresheim, 2006). A best fit and an average value of OH was computed

311   separately for both toluene and C8 aromatics according to Eq. (3) (shown in Fig. 3). Results are

312   included in Table 2. The average of these two values was used as the concentration of OH in further

313   analysis.

314

315   Using this [OH], the k_{OH} for C9 and C10 aromatics were allowed to vary. Best fits for the C9 and

316   C10 aromatics were calculated and are shown in Fig. 3. The group average rate constants (Table

317   2) are within the range of values known for isomers of C9 and C10 aromatics. For C9 aromatics,

318   the group average rate constant was determined to be 16.9 cm^3 molecule^{-1} s^{-1}; known values range

319   from 5.3 (n-propylbenzene) to 56.7 cm^3 molecule^{-1} s^{-1} (1,3,5-trimethylbenzene) (Atkinson and

320   Arey, 2003). For C10 aromatics, the group average rate constant was determined to be 24.2 cm^3

321   molecule^{-1} s^{-1}; known values range from 4.5 (t-butylbenzene) (Atkinson and Arey, 2003) to 55.5

322   cm^3 molecule^{-1} s^{-1} (1,2,4,5-tetramethylbenzene) (Aschmann et al., 2013). The average rate constant

323   constrains group composition, and could be useful in future investigations of photochemical

324   processing.

325

326   Knowledge of typical daily OH concentrations is crucial to understand photochemical processing

327   of VOCs and ozone production. OH was not measured directly in 2013, but our analysis provides

328   an estimate of OH exposure that is constrained by solar actinic flux and VOC measurements. OH

329   peaked daily at 1×10^6 ($\pm 21\%$) molecule cm^{-3}, which is low compared to urban areas affected by

330   photochemical smog with typical OH concentrations between $(5-10) \times 10^6$ molecule cm^{-3} (Shirley

331   et al., 2006). We compare to an independent estimate of [OH] in 2013 using the Master Chemical

332   Mechanism v.3.2 (MCM) framework (Edwards et al., 2014). The MCM OH estimate is generated

333   using more than 12000 explicit reactions comprising degradation schemes for nearly all

334   hydrocarbons measured at the Horse Pool site and has been applied previously to photochemistry

335   in the Uintah Basin (Edwards et al., 2014; Edwards et al., 2013). The agreement between our

336   model and the MCM estimate in peak daytime concentration is within a factor of 1.7 overall and

337   differs by only 2% on 5 Feb. 2013 (Fig. 7). The agreement is especially good considering that OH

338   values in our analysis are constrained by measured photolysis rates and a single scaling factor, and

339　so cannot generate the multi-day trend seen in the MCM calculation. This excellent agreement

340　substantiates the chemistry described by the MCM model.

341

342　**3.2 Oxygenated compounds**

343　Oxygenated compounds may also have photochemical sources. For these species, the change in

344　concentration with time is controlled by the production rate via photochemistry, loss to reaction

345　with OH, and first-order loss processes such as mixing, photolysis and deposition. The rate of

346　change can be written similarly to Eq. (1):

347　$\frac{d[VOC]}{dt} = Yield * k_{precursors}[OH][precursors] - k_{VOC}[OH][VOC] - D[VOC]$　　　　(4)

348　Here [precursors] is the sum concentration of all precursor species, *Yield* is the fraction of reactions

349　with OH that form the product compound, and $k_{precursors}$ is the weighted average OH rate constant

350　of precursor species. Again, D represents first-order loss processes. The oxygenated species

351　considered here are acetaldehyde, acetone, 2-butanone (MEK), formic acid, methanol, and

352　formaldehyde.

353

354　As with Eq. (2c), the rate of change of the ratio of a photochemically produced compound to

355　benzene is:

356　$\frac{d(ratio)}{dt} = Yield * k_{precursors}[OH] * R_{PB} - (ratio) * \left([OH]\left(k_{prod} - k_B\right) + J + \frac{P_B}{[B]}\right)$　　(5a)

357　　　　　　　$= \lambda_f * [OH] - (ratio) * \left([OH]\left(k_{prod} - k_B\right) + J + \frac{P_B}{[B]}\right)$　　　　　(5b)

358　R_{PB} is the ambient ratio of precursor species to benzene, k_{prod} and k_B are the OH rate constants of

359　the product species and benzene, and J is the photolysis rate constant of the product species. Here

360　we again assume that other first-order processes, mixing and deposition, are not significantly

361　different between the oxygenated VOCs and benzene. On the other hand, most of these compounds

362　contain a carbonyl functional group, and photolysis rates could be significant. J was set

363　proportional to solar actinic flux and scaled to photolysis constants from the literature (values and

364　literature sources are given in Table 3). We also assume that the only source of these species is

365　photochemistry; i.e. they are not emitted directly from primary sources. Methanol and

366　formaldehyde are included in this section as they are oxygenated species. However, the high

367　observed mixing ratios of methanol and formaldehyde (Table 1), previous modeling work

368　(Edwards et al., 2014), and knowledge of industry practices indicates that these two species also

369 have direct (primary) sources. We first analyzed methanol and formaldehyde assuming solely

370 photochemical sources, to investigate the extent to which secondary formation can explain their

371 behavior. We then modified the analysis to consider primary emission of these species. Methanol

372 and formaldehyde are discussed separately in the analysis (below).

373

374 As the relative amounts of precursor species and their product yields were unknown, *yield,*

375 $k_{precursors}$, and R_{PB} were bundled into a single free variable, λ_f (formation rate constant). The term

376 R_{PB} requires further discussion. The analysis of primary compounds (above) shows that the ratios

377 of C7-C10 aromatics to benzene are highly variable and depend on photochemical exposure. $R_{PB,}$

378 the ratio of precursor species to benzene, should also change over time. However, in applying

379 Equation (5b), we have simplified analysis by treating R_{PB} as approximately constant. By volume,

380 the dominant VOCs measured at Horse Pool were C1-C5 alkanes. These compounds react more

381 slowly with OH than C7-C10 aromatics. Reaction with OH has a proportionally smaller effect on

382 their concentrations, and indeed, ratios of these compounds to benzene show less diurnal

383 variability (Fig. 8a). Despite how slowly these compounds react with OH, the very large

384 concentration of these compounds means that C2-C5 alkanes account for most of the reactions

385 between OH and VOCs, and are the most important precursor compounds (Fig. 8b). We can

386 therefore use the simplifying approximation of constant precursor:benzene ratio.

387

388 Again, the analysis was first applied to night data only. During the night, (5b) reduces to:

389 $$\frac{d(ratio)}{dt} = -(ratio)\left(\frac{P_B}{[B]}\right) \tag{6}$$

390 Using Equation (6), a best fit was calculated for acetaldehyde, formic acid, acetone, MEK,

391 methanol, and formaldehyde (Fig. 9), providing six values of the primary benzene emission rate

392 (P_B) (Table 3).

393

394 The best fit functions to acetone, acetaldehyde, formic acid, and MEK for nighttime data only were

395 able to predict a decreasing trend in the ratio of VOC:benzene, but did not replicate the strong

396 decrease in ratio towards the end of the night. Primary emission of benzene during the night could

397 only account for a portion of the decrease, signifying an additional oxygenate removal process not

398 included in Equation (6). A possible candidate is increased deposition of oxygenates. Including a

399 free first-order deposition variable did not significantly affect model output, suggesting a complex

400 process increasing in strength during the night. One possibility is deposition on ice crystals.
401 Surfaces, including the sampling inlet, typically gained a thick coating of ice rime during the night,
402 creating additional surface area available for deposition. This process would also affect polar
403 oxygenated species much more than primary hydrocarbons, consistent with the additional decrease
404 in oxygenates not observed with aromatics. Because this process affected our sampling inlet, it is
405 possible that oxygenate behavior during early morning is an inlet artifact rather than a significant
406 basin-wide process. We removed rime ice from the sampling inlet early each morning, and other
407 surfaces were typically free of rime by mid-morning (snow cover remained during the day).

408

409 The values of benzene emission rate derived from night-only best fit to acetone, acetaldehyde,
410 formic acid, and MEK were slightly higher than estimates from primary compounds: 5×10^5 as
411 opposed to 4×10^5 molecule cm^{-3} s^{-1}. This is consistent with an undetermined additional removal
412 process. In the absence of an appropriate loss term, a best fit using Equation (6) would artificially
413 increase the benzene emission rate to reproduce the stronger downwards trend in ratio.

414

415 The diurnal behaviors of methanol and formaldehyde differ significantly from other species. The
416 ratios of methanol and formaldehyde to benzene do not increase steadily during the day and do not
417 decrease at night. Additionally, the values of primary benzene emission rate determined from
418 methanol and formaldehyde are at least a factor of two smaller than values determined from any
419 other compound. For methanol, this behavior is almost certainly due to large primary sources.
420 Methanol is used by the oil and natural gas industry in a variety of applications in the basin
421 (Lyman, 2014), including storage of methanol containers on wellpads, and direct emissions of
422 methanol associated with this use are very high as witnessed by hourly average mixing ratios in
423 the basin, which can build up to more than 200 ppbv. It is therefore unsurprising that methanol
424 variation is poorly described by Equation (6). Primary sources of formaldehyde are less clear.
425 Incomplete combustion and emission from dehydrators, separators, compressors, flares, oil pumps
426 and processing plants have been suggested as sources, but are not well quantified in the Uintah
427 basin. Additionally, there is no easily distinguishable correlation between formaldehyde and NO_x,
428 so it is not clear that combustion is a significant source of formaldehyde. In accordance with our
429 findings, Edwards et al. (2014) left the option open for primary emissions of formaldehyde due to
430 the inability of the MCM model to reproduce the ambient mixing ratios.

431

432   To investigate primary emission of methanol and formaldehyde we modified Equation (6) in

433   several ways. First, we added a term representing primary emission of oxygenates and determined

434   best-fit values of benzene emission rate and oxygenate:benzene emission ratio. χ^2 values decreased

435   insignificantly (-5%, methanol) and slightly (-22%, formaldehyde) and calculated values of

436   primary benzene emission rate were unreasonable (8×10^5 and 1×10^6 molecules cm^{-3} s^{-1} from the

437   methanol and formaldehyde analysis, respectively). Next, we fixed the primary benzene emission

438   rate to the value determined from the primary compounds analysis and determined emission ratios

439   for methanol and formaldehyde only. Emission ratios of formaldehyde:benzene and

440   methanol:benzene were 1.01 and 10.3. These values are slightly less than the ambient ratios,

441   consistent with accumulation from both photochemistry and primary emission. However, the best

442   fit still did not capture the majority of measurement variability and may not be accurately

443   characterizing physical processes affecting methanol or formaldehyde. For instance, an emission

444   source poorly correlated with benzene would not be well represented by Equation (6).

445

446   Because of possible complex deposition of oxygenated species during the night, and primary

447   emission of methanol and formaldehyde, emission rates derived from the analysis of these

448   oxygenates are less likely to be accurate than those derived from analysis of primary species. We

449   elected to exclude night data from further analysis, and retain the primary benzene emission rate

450   (P_B) determined from the primary compounds model. The fit of Equation (5b) was then calculated

451   for acetone, MEK, acetaldehyde, and formic acid, using daytime data (Fig. 9), to determine values

452   of the formation rate constant (λ_f) for each compound (Table 3).

453

454   The best-fit of daytime oxygenate ratios is better able to explain the measurements, with R^2 values

455   of 0.4 to 0.8 (Table 3). Values of the formation rate constant (λ_f) are plausible. For instance, the

456   best-fit value of λ_f for acetone is 8.72×10^{-11} cm^3 molecule^{-1} s^{-1}. The main precursors of acetone

457   present in the Uintah Basin were iso-butane and propane. The weighted average rate constant for

458   reaction of iso-butane and propane with OH is 1.3×10^{-12} cm^3 molecule^{-1} s^{-1} and the mol ratio of

459   these compounds to benzene was approximately 70. Assuming that all propane-OH and iso-

460   butane-OH reactions formed acetone, the calculated λ_f for acetone is 9.1×10^{-11} cm^3 molecule^{-1} s^{-1},

461   which is very close to the best-fit calculated value. The high R^2 values and reasonable λ_f suggest

462   that Equation (5b) captures the most important daytime processes affecting acetone, acetaldehyde,

463   MEK, and formic acid.

464

465   **4. Organic carbon budget**

466   In this section, we categorize VOCs as either primary (directly emitted) or secondary (enhanced by

467   oxidative chemistry), and quantify the total organic carbon mass in each category. Using two

468   complementary mass balance approaches, we show that one would expect to see more oxygenated species

469   than were measured. Both approaches rely on conservation of organic carbon mass: when a primary

470   compound is oxidized, the total mass of organic carbon does not change. This is true regardless if

471   the molecule's structure changes, if it fragments into several smaller molecules, if subsequent

472   reactions form higher generation products, or if it moves into a different reservoir (e.g. aerosol or

473   snowpack).

474

475   First, carbon mass concentration is conserved. The total organic carbon mass of primary compounds

476   lost to oxidation must be equal to the total organic carbon mass gained by secondary compounds.

477   To quantify this mass, we use the loss rate of a primary compound to oxidation:

478    $$\frac{d(primary\ VOC)}{dt}\bigg|_{chemical} = -k_{PrimaryVOC}[OH][primary\ VOC] \qquad (7)$$

479   The amount of organic carbon lost from all primary species measured by PTR-MS and GC-FID

480   (compounds listed in Table 1) during the stagnation event can be found by integrating Equation

481   (7) for each individual primary VOC, then summing the results over all primary VOCs. For

482   completeness, methane (from CaRDS) was also included. [OH] was set to the values calculated

483   above (Table 2). OH rate constants for C8, C9, and C10 aromatics were taken from Table 2, and

484   OH rate constants for all other species were taken from Atkinson and Arey, 2003.

485

486   Because total carbon mass is conserved, the total carbon mass lost from primary species is equal

487   to the total carbon mass gained by all secondary species. This value, about 3.7×10^{-10} gram C cm^{-3}

488   on day 6 of the stagnation event, is the calculated or expected mass of secondary species. Measured

489   oxygenates and secondary species, including methanol, formaldehyde, formic acid, acetone,

490   acetaldehyde, MEK, PAN species (peroxyacrylic nitric anhydride (APAN), peroxymethacrylic

491   nitric anhydride (MPAN), peroxyacetic nitric anhydride (PAN), and peroxypropionic nitric

492 anhydride (PPN)), organic carbon in snow, and PM2.5 organic aerosol, only sum to 0.64×10^{-10}

493 gram C cm^{-3}, or 17% of calculated secondary carbon mass.

494

495 Methanol and formaldehyde have substantial primary sources, so including them in this calculation

496 artificially increases the percentage of secondary species accounted for: 0.64×10^{-10} gram C cm^{-3} is

497 an upper bound to the mass of measured secondary species. If we assume methanol is entirely

498 primary, measured secondary species only sum to 0.48×10^{-10} gram C cm^{-3}, or 12.9% of calculated

499 secondary carbon mass. If we assume both methanol and formaldehyde have no photochemical

500 sources, measured secondary species sum to 0.46×10^{-10} gram C cm^{-3}, or 12.5% of calculated

501 secondary carbon mass. Figure 10 shows the upper bound to measured secondary species

502 (including both methanol and formaldehyde).

503

504 This gap between the calculated (expected) mass of secondary species and the measured mass of

505 secondary species is a factor of 5.8 (Fig. 10). Other measurement and modeling studies of the

506 Uintah Basin suggest that unquantified secondary species are responsible for a large part of this

507 gap: many additional oxygenated VOCs were detected, but not quantified, by PTR-time-of-flight

508 (PTR-ToF) mass spectrometry (Warneke et al., 2015), and MCM modeling indicates that carbonyl

509 groups formed from higher-weight species (e.g. aromatics) were not only abundant but major

510 drivers of ozone formation.

511

512 Oxidation of quantified secondary species to CO and CO_2, or loss to mixing out of the basin are

513 alternate explanations that could account for some of the disparity. Using a second carbon mass

514 balance technique, we show that unquantified secondary species are an important factor. The

515 second technique compares oxidation rates: the oxidation loss rate of primary species must be

516 equal to the photochemical formation rate of secondary species. Neither of these processes is

517 affected by higher-generation oxidation reactions or loss to mixing or deposition. A disparity

518 between the carbon mass loss rate to oxidation of primary species and the formation rate of

519 measured secondary species means that there must be other, unquantified, secondary species

520 forming. Therefore, comparing oxidation and formation rates provides a way to determine if the

521 mass disparity between calculated and measured secondary species is at least partly due to

522 unquantified compounds.

17

523

524   The total oxidation rate of primary species was determined by applying Equation (7) to each

525   measured primary species, then summing over all primary species. The formation rate of quantified

526   secondary species was determined using Equation (4). The first term in Equation (4),

527    $Yield * k_{precursors}[OH][precursors]$, is the formation rate of a secondary VOC. To clarify, this

528   is the rate at which a secondary VOC is produced by oxidation chemistry, not the rate of net

529   increase in mass (net = formation – loss). As in Equation (5b), this can be simplified to

530    $$\left.\frac{d(secondary\ VOC)}{dt}\right|_{formation} = \lambda_f[OH][benzene] \qquad (8a)$$

531    $$\lambda_f = Yield * k_{precursors} * \frac{[precursors]}{[benzene]} \qquad (8b)$$

532   λ_f is the formation rate constant, and was (above) determined for acetone, acetaldehyde, formic

533   acid, and MEK. The oxidation rate of primary compounds is a factor of two higher than the

534   formation rate of acetaldehyde, acetone, formic acid, and MEK (Fig. 11). This large disparity

535   indicates a substantial presence of unquantified secondary species. The formation rate of these

536   species is $3.2(\pm 1.2) \times 10^{-16}$ g C cm^{-3} s^{-1} on average or $60(\pm 23)$ ppbv C day^{-1}.

537

538   **5. Conclusions**

539   High concentrations of organic carbon species (up to 5 ppm nonmethane carbon) associated with

540   oil and natural gas extraction were measured at a rural site in the Uintah Basin, Utah, during the

541   winter of 2013. A relatively simple analysis was applied to measurements of aromatic species by

542   PTRMS to explain variation in their ratios due to reaction with OH and primary emission. The

543   analysis was extended to measurements of small oxygenated compounds by PTRMS, with the goal

544   of explaining ratios of these compounds to benzene in terms of production and loss via OH

545   chemistry, photolysis, and primary emission. Results of both analyses were used to develop a

546   carbon mass budget, to determine the relative fractions of carbon in primary and secondary species.

547

548   The analysis of primary aromatic species provided plausible estimates of [OH], aromatic VOC

549   emission ratios, and benzene emission rate. The daily peak of [OH] was low (1×10^6 molecule cm$^-$

550   ^{3}), consistent with MCM modeling and highlighting the unusual oxidation chemistry occurring in

551   this region. Emission ratios indicate source contributions from both oil and gas wells. Using

552   measured correlation between benzene and methane, the benzene emission rate ($4.1 \pm 0.4 \times 10^5$

553 molecule cm^{-3} s^{-1}) was extrapolated to a basin-wide methane emission rate ($27\text{-}57x10^3$ kg methane

554 hr^{-1}) in order to compare with an independent top-down estimate from aircraft. Although the large

555 uncertainties associated with the extrapolation of the benzene emission rate to a basin-wide

556 methane emission rate preclude the use of our estimate as an assessment of regulatory inventories,

557 the agreement with the 2012 aircraft methane flux value supports the plausibility of our analysis.

558 Our analysis was not able to completely explain night time variability of small oxygenated VOCs,

559 whose behavior may be affected by primary emission (methanol and formaldehyde) and deposition

560 to ice surfaces. However, a best fit to day time data provided values of carbonyl formation rate

561 consistent with expected formation rates from known precursors. The calculated carbon budget

562 indicated that a large fraction of secondary carbon mass (83%, or $3x10^{-10}$ gC cm^{-3}) is unaccounted

563 for. A comparison of measured carbonyl formation rates to primary compound oxidation rates

564 indicated substantial presence of unquantified secondary species.

565

566 The analysis method outlined here is relatively simple, including just a few terms for basic

567 chemistry and primary emission. It uses little computer processing power and references only

568 measurements that can be made with standard VOC instrumentation. Despite its simplicity, this

569 method is able to provide considerable information on VOC chemistry, including source

570 composition and emission rates, the concentration of OH, and measurement thoroughness. Best-

571 fit values are very reasonable and support findings from more complicated chemical models. A

572 similar analysis could be applied to investigations of other regions where VOC pollutants are

573 geographically or meteorologically contained, especially where detailed chemical measurements

574 are unavailable or not possible.

575

References

Adgate, J. L., Goldstein, B. D., and McKenzie, L. M.: Potential public health hazards, exposures and health effects from unconventional natural gas development, Environ. Sci. Technol., 48, 8307-8320, 10.1021/es404621d, 2014.

Allen, D. T., Torres, V. M., Thomas, J., Sullivan, D. W., Harrison, M., Hendler, A., Herndon, S. C., Kolb, C. E., Fraser, M. P., Hill, A. D., Lamb, B. K., Miskimins, J., Sawyer, R. F., and Seinfeld, J. H.: Measurements of methane emissions at natural gas production sites in the United States, P. Natl. Acad. Sci. USA, 110, 17768-17773, 10.1073/pnas.1304880110, 2013.

Anglada, J. M.: Complex Mechanism of the Gas Phase Reaction between Formic Acid and Hydroxyl Radical. Proton Coupled Electron Transfer versus Radical Hydrogen Abstraction Mechanisms, Am. Chem. Soc., 126, 9809-9820, 10.1021/ja0481169, 2004.

Aschmann, S. M., Arey, J., and Atkinson, R.: Rate Constants for the Reactions of OH Radicals with 1,2,4,5-Tetramethylbenzene, Pentamethylbenzene, 2,4,5-Trimethylbenzaldehyde, 2,4,5-Trimethylphenol, and 3-Methyl-3-hexene-2,5-dione and Products of OH + 1,2,4,5-Tetramethylbenzene, J. Phys. Chem. A, 117, 2556-2568, 10.1021/jp400323n, 2013.

Atkinson, R., and Arey, J.: Atmospheric degradation of volatile organic compounds, Chem. Rev., 103, 4605-4638, 2003.

Bates, T. S., Quinn, P. K., Coffman, D. J., Covert, D. S., Miller, T. L., Johnson, J. E., Carmichael, G. R., Uno, I., Guazzotti, S. A., Sodeman, D. A., Prather, K. A., Rivera, M., Russell, L. M., and Merrill, J. T.: Marine boundary layer dust and pollutant transport associated with the passage of a frontal system over eastern Asia, J. Geophys. Res: Atmos., 109, D19S19, 10.1029/2003JD004094, 2004.

Brandt, A. R., Heath, G. A., Kort, E. A., O'Sullivan, F., Pétron, G., Jordaan, S. M., Tans, P., Wilcox, J., Gopstein, A. M., Arent, D., Wofsy, S., Brown, N. J., Bradley, R., Stucky, G. D., Eardley, D., and Harriss, R.: Methane Leaks from North American Natural Gas Systems, Science, 343, 733-735, 2014.

Carter, W. P. L., and Seinfeld, J. H.: Winter ozone formation and VOC incremental reactivities in the Upper Green River Basin of Wyoming, Atmos. Env., 50, 255-266, 10.1016/j.atmosenv.2011.12.025, 2012.

Crosson, E. R.: A cavity ring-down analyzer for measuring atmospheric levels of methane, carbon dioxide, and water vapor, Appl. Phys. B, 92, 403-408, 10.1007/s00340-008-3135-y, 2008.

de Gouw, J., and Warneke, C.: Measurements of volatile organic compounds in the earth's atmosphere using proton-transfer-reaction mass spectrometry, Mass. Spectrom. Rev., 26, 223-257, 10.1002/mas.20119, 2007.

de Gouw, J. A., Middlebrook, A. M., Warneke, C., Goldan, P. D., Kuster, W. C., Roberts, J. M., Fehsenfeld, F. C., Worsnop, D. R., Canagaratna, M. R., Pszenny, A. A. P., Keene, W. C., Marchewka, M., Bertman, S. B., and Bates, T. S.: Budget of organic carbon in a polluted atmosphere: Results from the New England Air Quality Study in 2002, J. Geophys. Res.: Atmos., 110, D16305, 10.1029/2004JD005623, 2005.

Edwards, P. M., Brown, S. S., Roberts, J. M., Ahmadov, R., Banta, R. M., deGouw, J. A., Dube, W. P., Field, R. A., Flynn, J. H., Gilman, J. B., Graus, M., Helmig, D., Koss, A., Langford, A. O., Lefer, B. L., Lerner, B. M., Li, R., Li, S.-M., McKeen, S. A., Murphy, S. M., Parrish, D. D., Senff, C. J., Soltis, J., Stutz, J., Sweeney, C., Thompson, C. R., Trainer, M. K., Tsai, C., Veres, P. R., Washenfelder, R. A., Warneke, C., Wild, R. J., Young, C. J., Yuan, B., and Zamora, R.: High winter ozone pollution from carbonyl photolysis in an oil and gas basin, Nature, 514, 351-354, 10.1038/nature13767, 2014.

Edwards, P. M., Young, C. J., Aikin, K., deGouw, J., Dubé, W. P., Geiger, F., Gilman, J., Helmig, D., Holloway, J. S., Kercher, J., Lerner, B., Martin, R., McLaren, R., Parrish, D. D., Peischl, J., Roberts, J. M., Ryerson, T. B., Thornton, J., Warneke, C., Williams, E. J., and Brown, S. S.: Ozone photochemistry in an oil and natural gas extraction region during winter: simulations of a snow-free season in the Uintah Basin, Utah, Atmos. Chem. Phys., 13, 8955-8971, 10.5194/acp-13-8955-2013, 2013.

Etzkorn, T., Klotz, B., Sørensen, S., Barnes, I., Becker, K. H., and Platt, U.: Gas-phase absorption cross sections of 24 monocyclic aromatic hydrocarbons in the UV and IR spectral ranges, Atmos. Env., 33, 525 - 540, 10.1016/S1352-2310(98)00289-1, 1999.

Gilman, J. B., Burkhart, J. F., Lerner, B. M., Williams, E. J., Kuster, W. C., Goldan, P. D., Murphy, P. C., Warneke, C., Fowler, C., Montzka, S. A., Miller, B. R., Miller, L., Oltmans, S. J., Ryerson, T. B., Cooper, O. R., Stohl, A., and de Gouw, J. A.: Ozone variability and halogen oxidation within the Arctic and sub-Arctic springtime boundary layer, Atmos. Chem. Phys., 10, 10223-10236, 10.5194/acp-10-10223-2010, 2010.

Gilman, J. B., Lerner, B. M., Kuster, W. C., and de Gouw, J. A.: Source signature of volatile organic compounds from oil and natural gas operations in northeastern Colorado, Environ. Sci. Technol., 47, 1297-1305, 10.1021/es304119a, 2013.

Hard, T. M., Chan, C. Y., Mehrabzadeh, A. A., Pan, W. H., and O'Brien, R. J.: Diurnal cycle of tropospheric OH, Nature, 322, 617-620, 1986.

Helmig, D., Thompson, C. R., Evans, J., Boylan, P., Hueber, J., and Park, J. H.: Highly Elevated Atmospheric Levels of Volatile Organic Compounds in the Uintah Basin, Utah, 48, 4707-4715, 10.1021/es405046r, 2014.

Jobson, B. T., Niki, H., Yokouchi, Y., Bottenheim, J., Hopper, F., and Leaitch, R.: Measurements of C2-C6 hydrocarbons during the Polar Sunrise 1992 Experiment: Evidence for Cl atom and Br atom chemistry, J. Geophys. Res.: Atmos., 99, 25355--25368, 10.1029/94JD01243, 1994.

Karion, A., Sweeney, C., Pétron, G., Frost, G., Michael Hardesty, R., Kofler, J., Miller, B. R., Newberger, T., Wolter, S., Banta, R., Brewer, A., Dlugokencky, E., Lang, P., Montzka, S. A., Schnell, R., Tans, P., Trainer, M., Zamora, R., and Conley, S.: Methane emissions estimate from airborne measurements over a western United States natural gas field, Geophys. Res. Lett., 40, 4393-4397, 10.1002/grl.50811, 2013.

Kotamarthi, V. R., and Holdridge, D. J.: Process-scale modeling of elevated wintertime ozone in Wyoming, Argonne National Laboratory, Argonne, IL, 2007.

Kuster, W. C., Jobson, B. T., Karl, T., Riemer, D., Apel, E., Goldan, P. D., and Fehsenfeld, F. C.: Intercomparison of Volatile Organic Carbon Measurement Techniques and Data at La Porte during the TexAQS2000 Air Quality Study, Environ. Sci. Technol., 38, 221-228, 10.1021/es034710r, 2004.

Li, R., Warneke, C., Graus, M., Field, R., Geiger, F., Veres, P. R., Soltis, J., Li, S.-M., Murphy, S. M., Sweeney, C., Pétron, G., Roberts, J. M., and de Gouw, J.: Measurements of hydrogen sulfide (H2S) using PTR-MS: calibration, humidity dependence, inter-comparison and results from field studies in an oil and gas production region, Atmos. Meas. Tech., 7, 3597-3610, doi:10.5194/amt-7-3597-2014, 2014.

Litovitz, A., Curtright, A., Abramzon, S., Burger, N., and Samaras, C.: Estimation of regional air-quality damages from Marcellus Shale natural gas extraction in Pennsylvania, Environ. Res. Lett., 8, 014017, 10.1088/1748-9326/8/1/014017, 2013.

Lyman, S.: Formaldehyde and Methanol Emission Sources in the Uinta Basin, Uinta Basin Winter Ozone Study 2014 Post Study Technical Meeting, Vernal, UT, 16-17 June 2014.

Martinez, R. D., Buitrago, A. A., Howell, N. W., Hearn, C. H., and Joens, J. A.: The near U.V. absorption spectra of several aliphatic aldehydes and ketones at 300 K, Atmos. Env. , 26, 785-792, http://dx.doi.org/10.1016/0960-1686(92)90238-G, 1992.

McKeen, S. A., Gierczak, T., Burkholder, J. B., Wennberg, P. O., Hanisco, T. F., Keim, E. R., Gao, R. S., Liu, S. C., Ravishankara, A. R., and Fahey, D. W.: The photochemistry of acetone in the upper troposphere: A source of odd-hydrogen radicals, Geophys. Res. Lett. , 24, 3177-3180, 10.1029/97gl03349, 1997.

Miller, S. M., Wofsy, S. C., Michalak, A. M., Kort, E. A., Andrews, A. E., Biraud, S. C., Dlugokencky, E. J., Eluszkiewicz, J., Fischer, M. L., Janssens-Maenhout, G., Miller, B. R., Miller, J. B., Montzka, S. A., Nehrkorn, T., and Sweeney, C.: Anthropogenic emissions of methane in the United States, P. Natl. Acad. Sci. USA, 110, 20018-20022, 10.1073/pnas.1314392110, 2013.

Moore, C. W., Zielinska, B., Pétron, G., and Jackson, R. B.: Air Impacts of Increased Natural Gas Acquisition, Processing, and Use: A Critical Review, Environ. Sci. Technol., 48, 8349-8359, 10.1021/es4053472, 2014.

Oltmans, S. J., Karion, A., Schnell, R. C., Pétron, G., Sweeney, C., Wolter, S., Neff, D., Montzka, S. A., Miller, B. R., Helmig, D., Johnson, B. J., and Hueber, J.: A high ozone episode in winter 2013 in the Uinta Basin oil and gas region characterized by aircraft measurements, Atmos. Chem. Phys. Discuss., 14, 20117-20157, 10.5194/acpd-14-20117-2014, 2014.

Roberts, J. M., Fehsenfeld, F. C., Liu, S. C., Bollinger, M. J., Hahn, C., Albritton, D. L., and Sievers, R. E.: Measurements of aromatic hydrocarbon ratios and NOx concentrations in the rural troposphere: Observation of air mass photochemical aging and NOx removal, Atmos. Env., 18, 2421-2432, http://dx.doi.org/10.1016/0004-6981(84)90012-X, 1984.

Rohrer, F., and Berresheim, H.: Strong correlation between levels of tropospheric hydroxyl radicals and solar ultraviolet radiation, Nature, 442, 184-187, 10.1038/nature04924, 2006.

Schnell, R. C., Oltmans, S. J., Neely, R. R., Endres, M. S., Molenar, J. V., and White, A. B.: Rapid photochemical production of ozone at high concentrations in a rural site during winter, Nature Geoscience, 2, 120-122, 10.1038/ngeo415, 2009.

Shirley, T. R., Brune, W. H., Ren, X., Mao, J., Lesher, R., Cardenas, B., Volkamer, R., Molina, L. T., Molina, M. J., Lamb, B., Velasco, E., Jobson, T., and Alexander, M.: Atmospheric oxidation in the Mexico City Metropolitan Area (MCMA) during April 2003, Atmos. Chem. Phys., 6, 2753-2765, 10.5194/acp-6-2753-2006, 2006.

Slusher, D. L., Huey, L. G., Tanner, D. J., Flocke, F. M., and Roberts, J. M.: A thermal dissociation–chemical ionization mass spectrometry (TD-CIMS) technique for the simultaneous measurement of peroxyacyl nitrates and dinitrogen pentoxide, J. Geophys. Res.: Atmos., 109, D19315, 10.1029/2004JD004670, 2004.

U.S. Energy Information Administration: May 2014 Monthly Energy Review, Washington, DC, 2014.

Utah Oil and Gas: http://oilgas.ogm.utah.gov/Data_Center/DataCenter.cfm, access: 3 June 2014.

Warneke, C., Geiger, F., Edwards, P. M., Dube, W., Pétron, G., Kofler, J., Zahn, A., Brown, S. S., Graus, M., Gilman, J. B., Lerner, B. M., Peischl, J., Ryerson, T. B., de Gouw, J. A., and Roberts, J. M.: Volatile organic compound emissions from the oil and natural gas industry in the Uintah Basin, Utah: oil and gas well pad emissions compared to ambient air composition, Atmos. Chem. Phys., 14, 10977-10988, 10.5194/acp-14-10977-2014, 2014.

Warneke, C., Veres, P., Murphy, S. M., Soltis, J., Field, R. A., Graus, M. G., Koss, A., Li, S.-M., Li, R., Yuan, B., Roberts, J. M., and de Gouw, J. A.: PTR-QMS versus PTR-TOF comparison in a region with oil and natural gas extraction industry in the Uintah Basin in 2013, Atmos.Meas. Tech., 8, 411–420, doi:10.5194/amt-8-411-2015, 2015.

Table 1. Compounds analyzed

PTR-MS Primary compounds	OH rate constant 10^{-12} cm^3 molecule^{-1} s^{-1}	Average mixing ratio ppbv (1 σ)	
Benzene	1.22	3.30	*(1.92)*
Toluene	5.63	4.00	*(2.76)*
C8 aromatics	16.4[a]	1.74	*(1.36)*
C9 aromatics	16.9[a]	0.365	*(0.271)*
C10 aromatics	24.2[a]	0.071	*(0.055)*
Secondary compounds			
Acetaldehyde	15.0	4.27	*(2.39)*
2-butanone (MEK)	1.22	2.81	*(1.69)*
Acetone	0.17	7.97	*(4.69)*
Formic acid	0.37[b]	2.56	*(1.43)*
Compounds with mixed or undetermined source			
Methanol	0.94	44.9	*(33.4)*
Formaldehyde	9.37	3.71	*(1.49)*
GC-FID Primary compounds			
Ethane	0.248	300	*(169)*
Propane	1.09	140	*(78.6)*
n-butane	2.36	48.0	*(26.9)*
2-methylpropane	2.12	30.3	*(17.1)*
n-pentane	3.80	18.8	*(10.5)*
2-methylbutane	3.60	20.9	*(11.8)*
2,2-dimethylpropane	0.825	0.306	*(0.181)*
n-hexane	5.20	8.32	*(4.65)*
Sum of 2- and 3-methylpentane	5.20	6.62	*(3.99)*
2,2-dimethylbutane	2.23	0.467	*(0.294)*
Methylcyclopentane	6.90	3.65	*(2.27)*
n-heptane	6.76	4.00	*(2.30)*
Methlcyclohexane	9.64	6.74	*(4.17)*
Ethyne	0.88	0.796	*(0.40)*
Ethene	8.52	2.05	*(1.06)*
Propene	26.3	0.171	*(0.0724)*

[a] Rate constants determined in this work.
[b] Anglada, 2004.
All other OH rate constants from Atkinson and Arey (2003).

Table 2. Primary compound results

Compound	Emission ratio to benzene *by mol*	Benzene emission rate 10^5 *molecule cm^{-3} s^{-1}*	[OH] avg. 10^5 *molecule cm^{-3}*	OH rate constant 10^{-12} *cm^3 molecule^{-1} s^{-1}*	R^2 – *full time series best fit*
Toluene	1.5	4.5	2.66	*5.63*	0.242

C8 aromatics	0.82	4.1	1.86	*16.4*	0.421
C9 aromatics	0.18	3.9		16.9	0.614
C10 aromatics	0.042	3.8		24.2	0.273

Table 2 includes results from the night-data only best fit (emission ratios, benzene emission rate), and the full time series (including both day and night) best fit ([OH], k_{OH}, and R^2).

Table 3. Oxygenated compound results

Compound	Benzene emission rate	Formation rate constant	R^2	Photolysis rate constant
	10^5 *molecule* cm^{-3} s^{-1}	10^{-11} cm^3 *molecule*$^{-1}$ s^{-1}	*(daytime data)*	s^{-1}
Acetaldehyde	4.91	7.36	0.667	1.2e-6 (Martinez et al., 1992)
Formic acid	6.04	3.30	0.414	1.0e-6 (estimated)
Acetone	4.46	8.72	0.775	5.0e-8 (McKeen et al., 1997)
MEK	4.97	3.42	0.787	3.6e-6 (Martinez et al., 1992)
Methanol	1.34			(day analysis not performed)
Formaldehyde	0.90			(day analysis not performed)

587
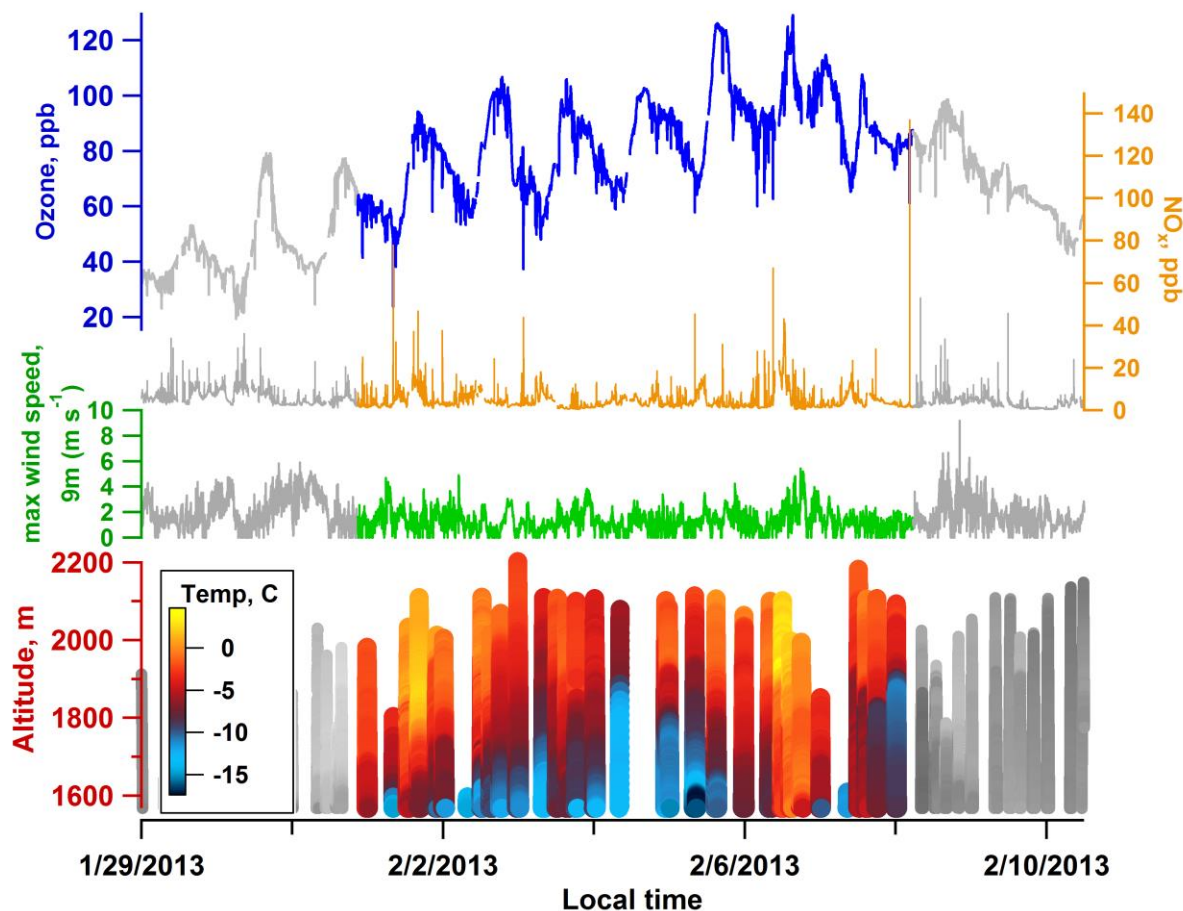
588 Figure 1. Ozone formation event and analysis period selection. The analyzed period (colored)
589 was selected to avoid high wind events on Jan 31 and Feb 8. (center) and include strong
590 temperature inversions (bottom) to minimize mixing of VOCs in or out of the basin.
591 Meteorological data courtesy of NOAA Physical Sciences Division. Temperature data from
592 tethered balloon sonde operated by NOAA Global Monitoring Division.
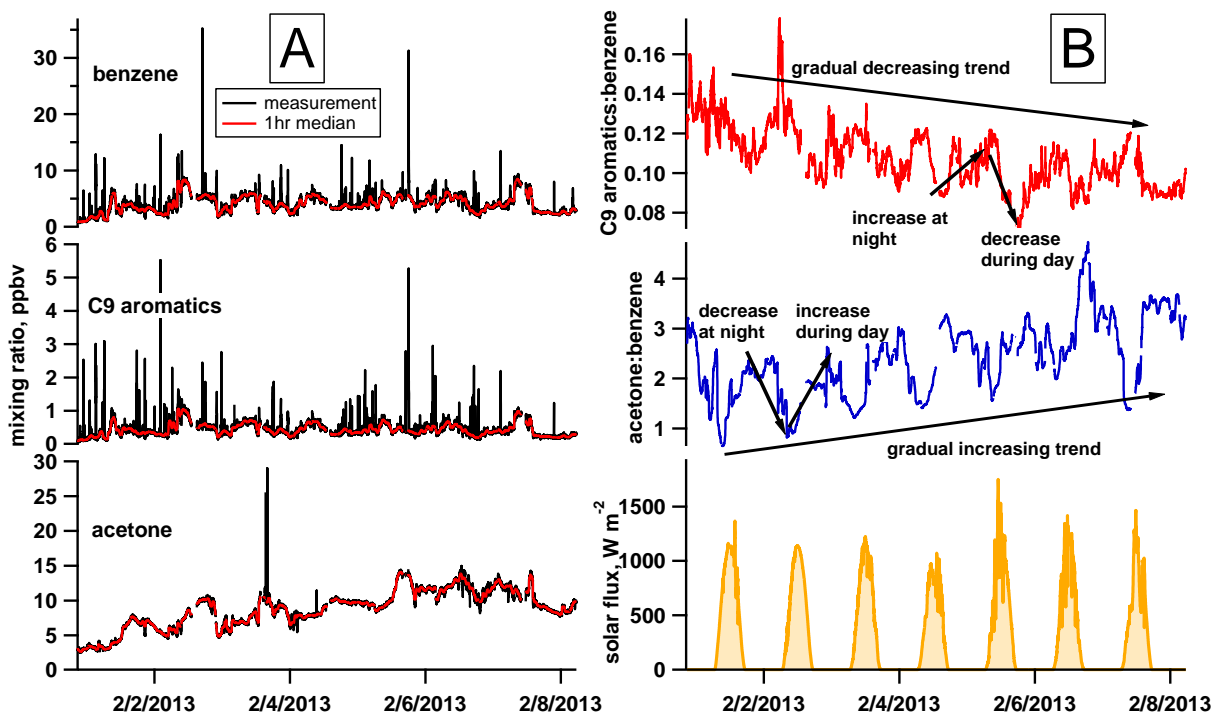
593
Figure 2. Description of trends in VOC concentrations and ratios. (A) Mixing ratios of
benzene, C9 aromatics, and acetone (black), and a one hour running median to isolate
spikes (red). (B) Ratios of C9 aromatics (top) and acetone (center) to benzene. Sunlight
intensity is shown beneath. The spikes visible in panel (A) have been removed to isolate
longer-term trends in VOC behavior (discussed in text).
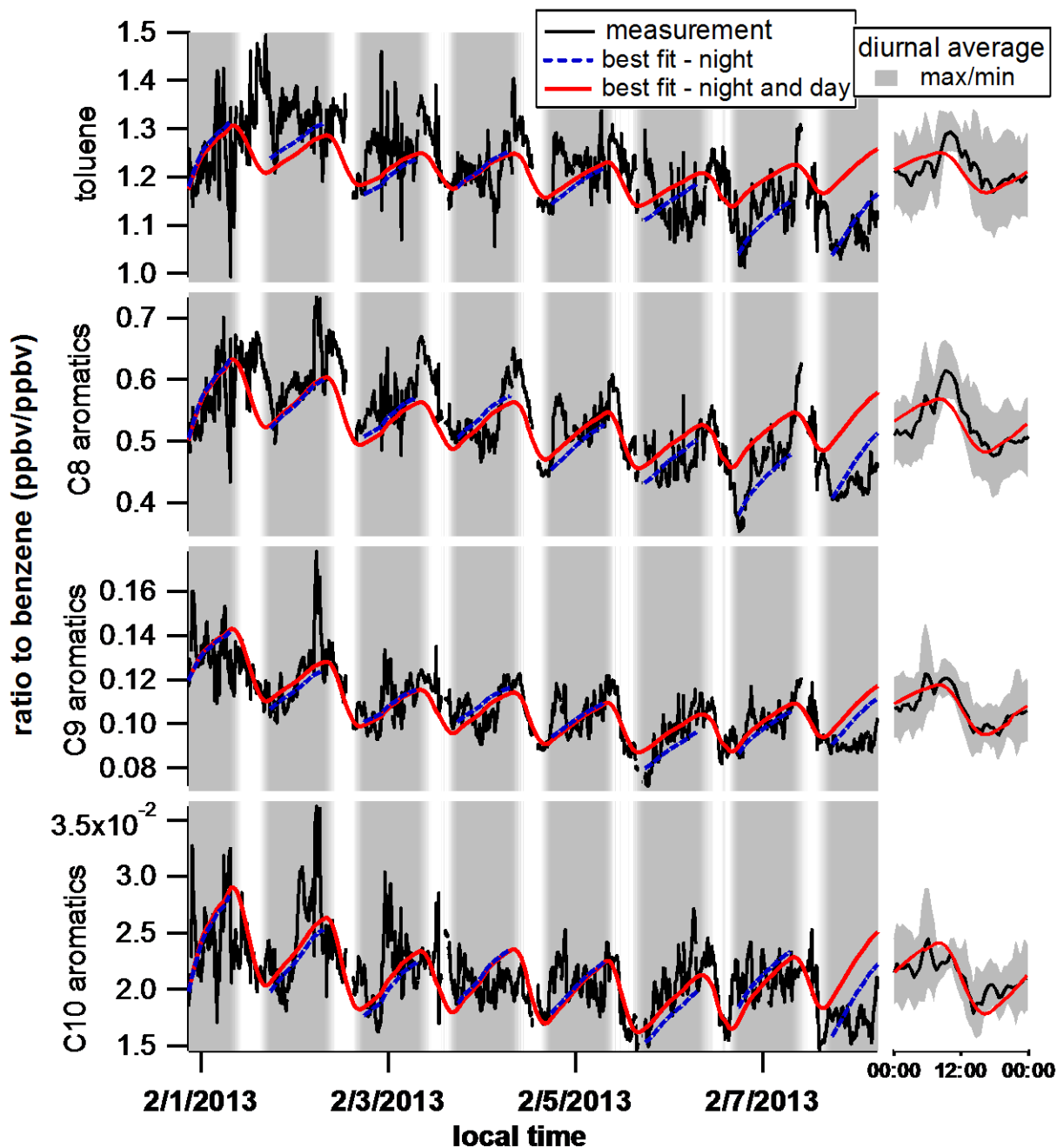
Figure 3. Aromatic compound ratios and best fit to night time data (blue) and both night and day data (red). The background is colored by sunlight intensity to distinguish day and night. For reproducibility, the initial ratio for each night was chosen from the 10th percentile of points during the first two hours of evening. In practice, best-fit parameters were largely insensitive to initial ratio, so long as the selected initial ratio was close to measurements during the early part of the night. A diurnal average is shown to the right.
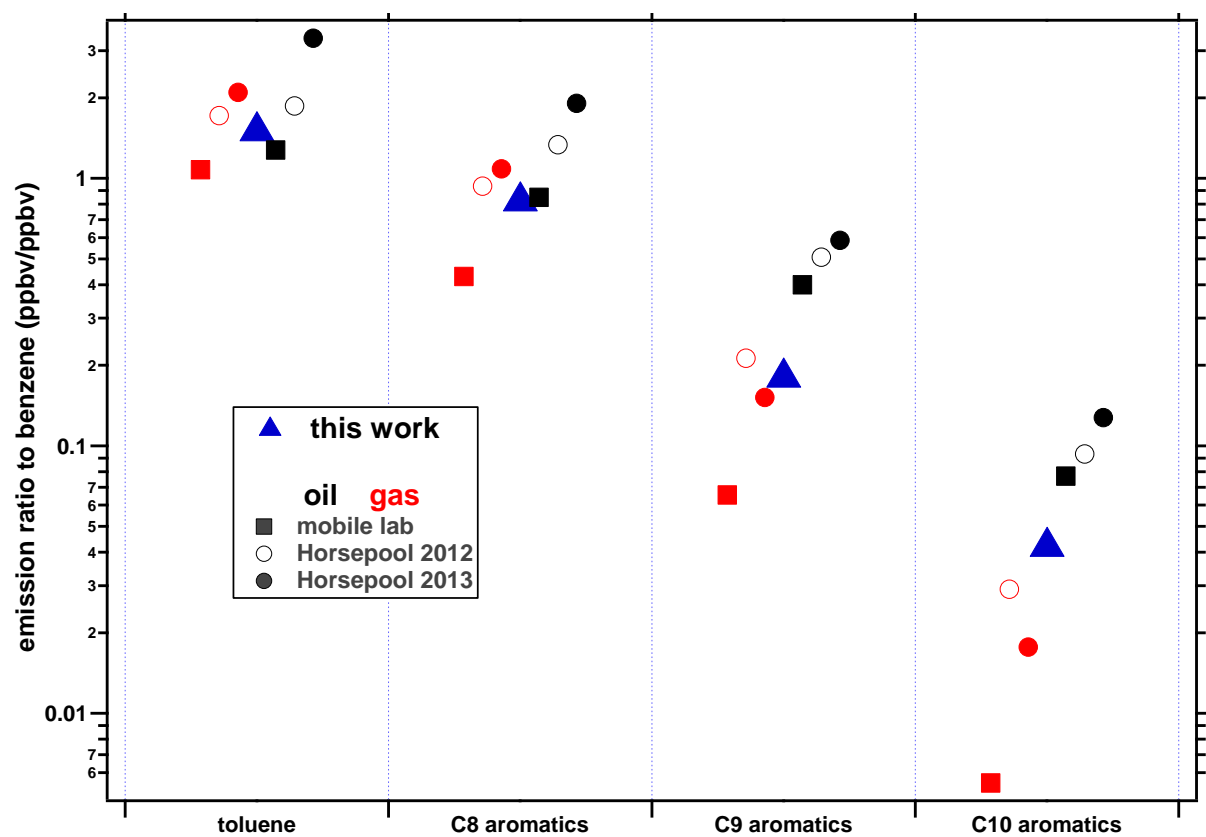
606
607 Figure 4. Comparison of emission ratio estimates. Emission ratio estimates from this analysis
608 (blue triangle) give an average emission ratio that is partway between the oil and gas
609 sources.
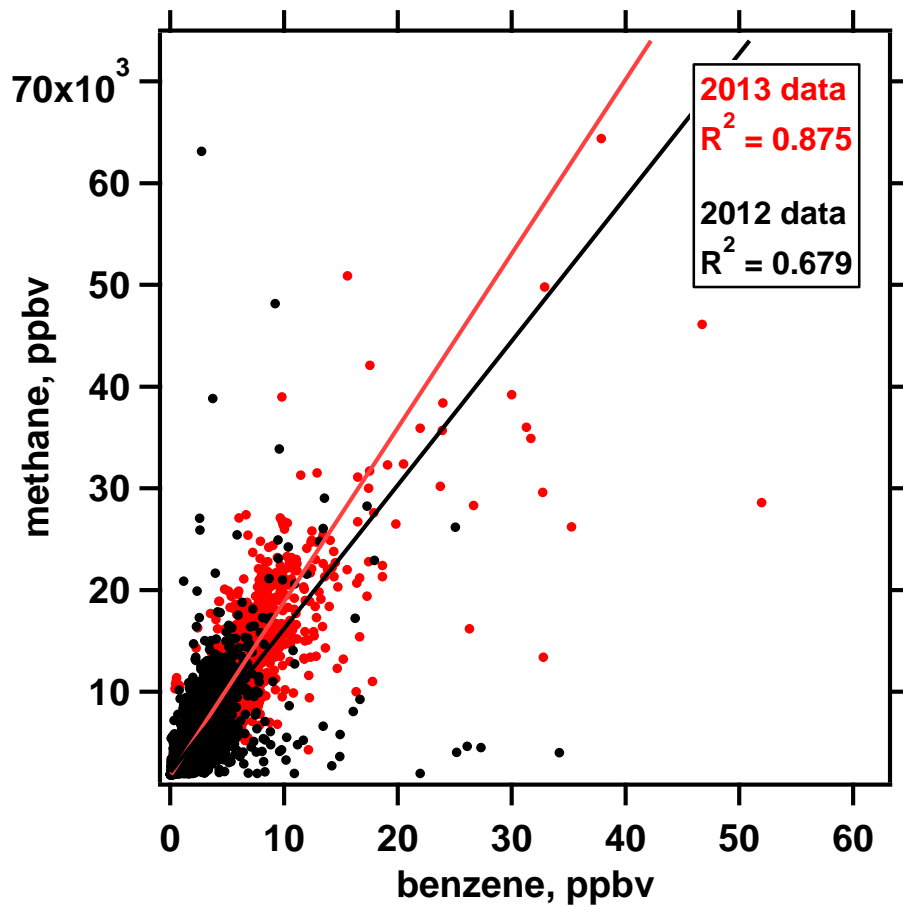
Figure 5. Correlation between methane and benzene for all data taken in 2013 (red) and 2012 (black).
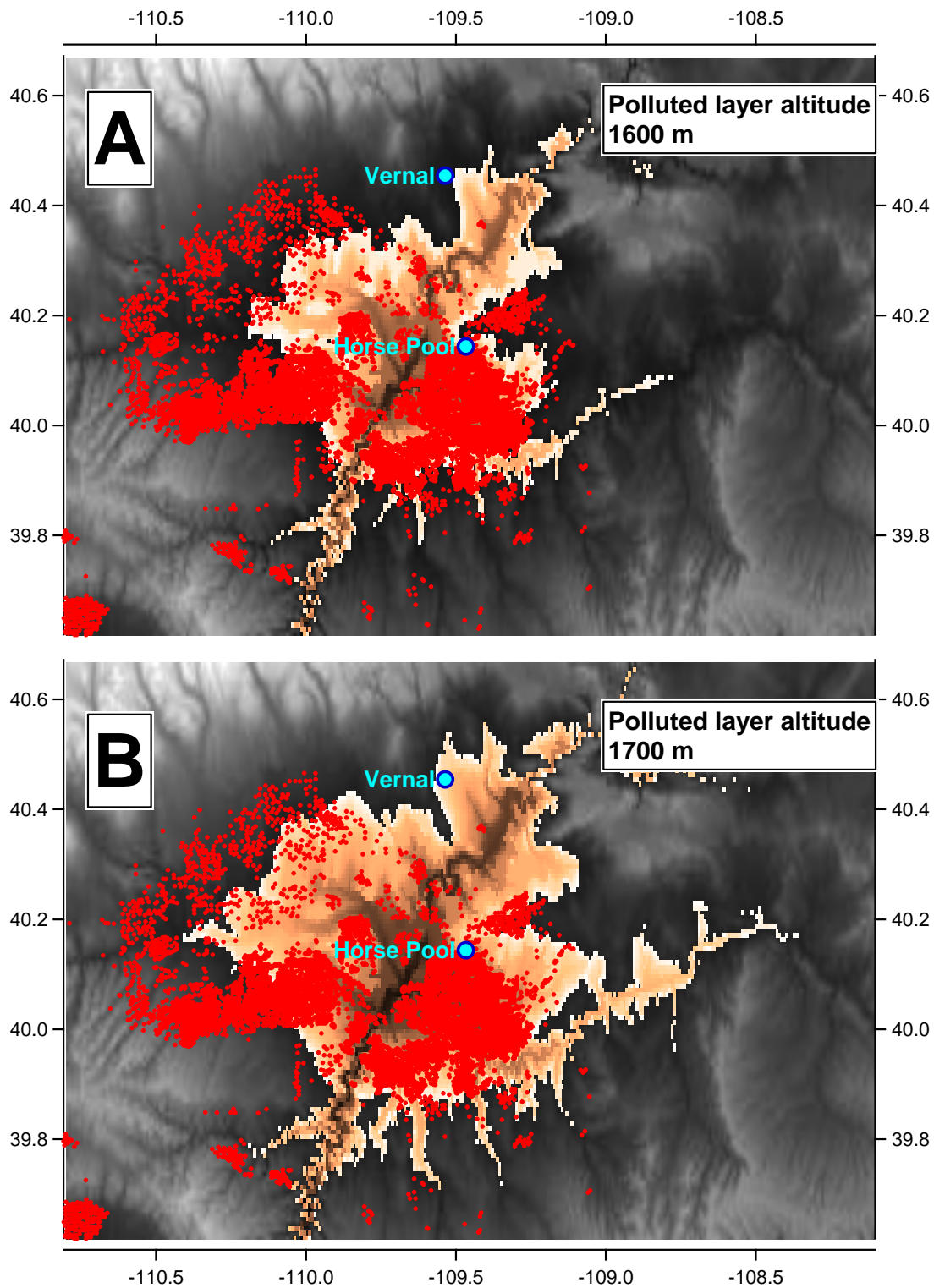
Figure 6. Topographical map of the Uintah Basin showing polluted region and well locations. Total relief is from 1398 meters above sea level to 3627m. The bright (tan) region shows the area of the polluted region assuming the polluted layer extends to 1600 meters above sea level (A) or 1700m (B). Locations of producing oil and gas wells are marked in red.
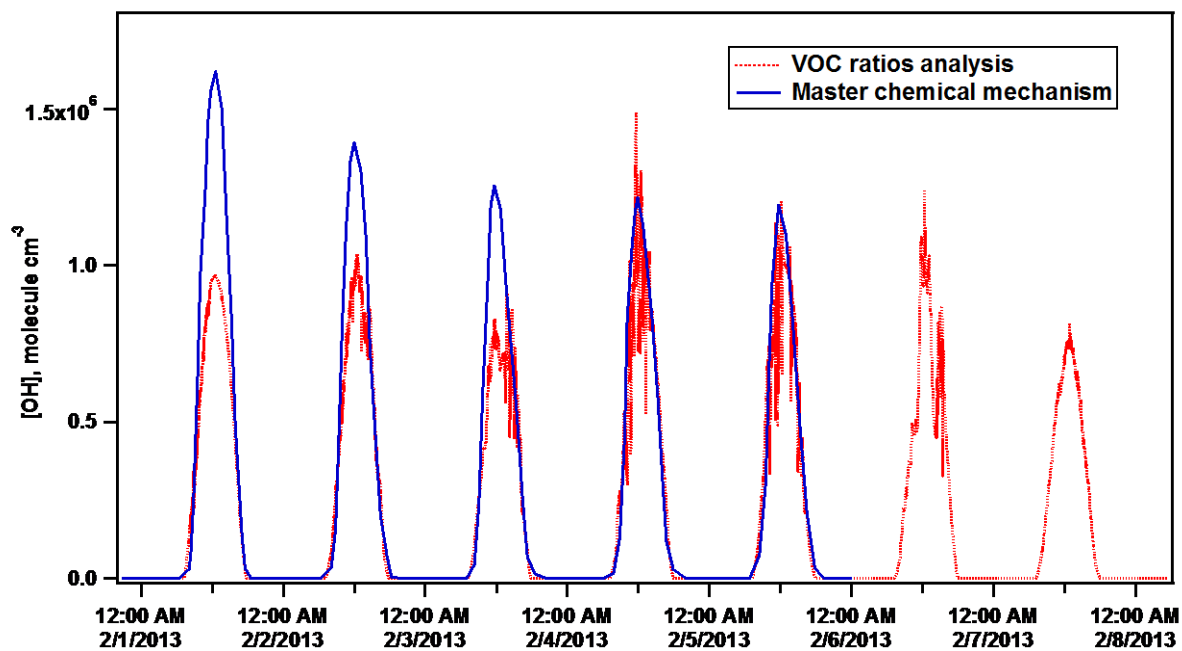
617   Figure 7. Comparison of OH with the Master Chemical Mechanism prediction. There is good
618   agreement between the MCM OH and OH determined from our analysis.
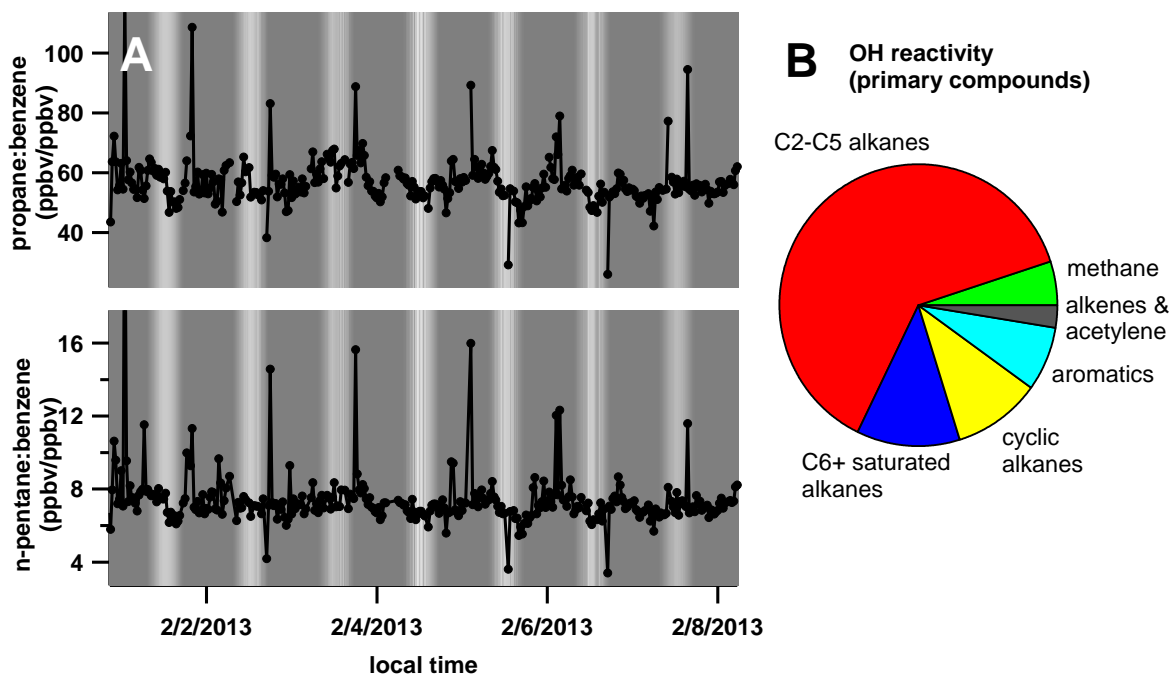
Figure 8. A. Because of their slow reaction rates with OH, the ratios of C2-C5 alkanes to benzene did not have high diurnal variability and did not change substantially from beginning to end of the stagnation event (propane and n-pentane measured by GC-FID are shown as representatives). B. However, because of their high mixing ratios, these species account for a large fraction (~70%) of primary hydrocarbon-OH reactions.
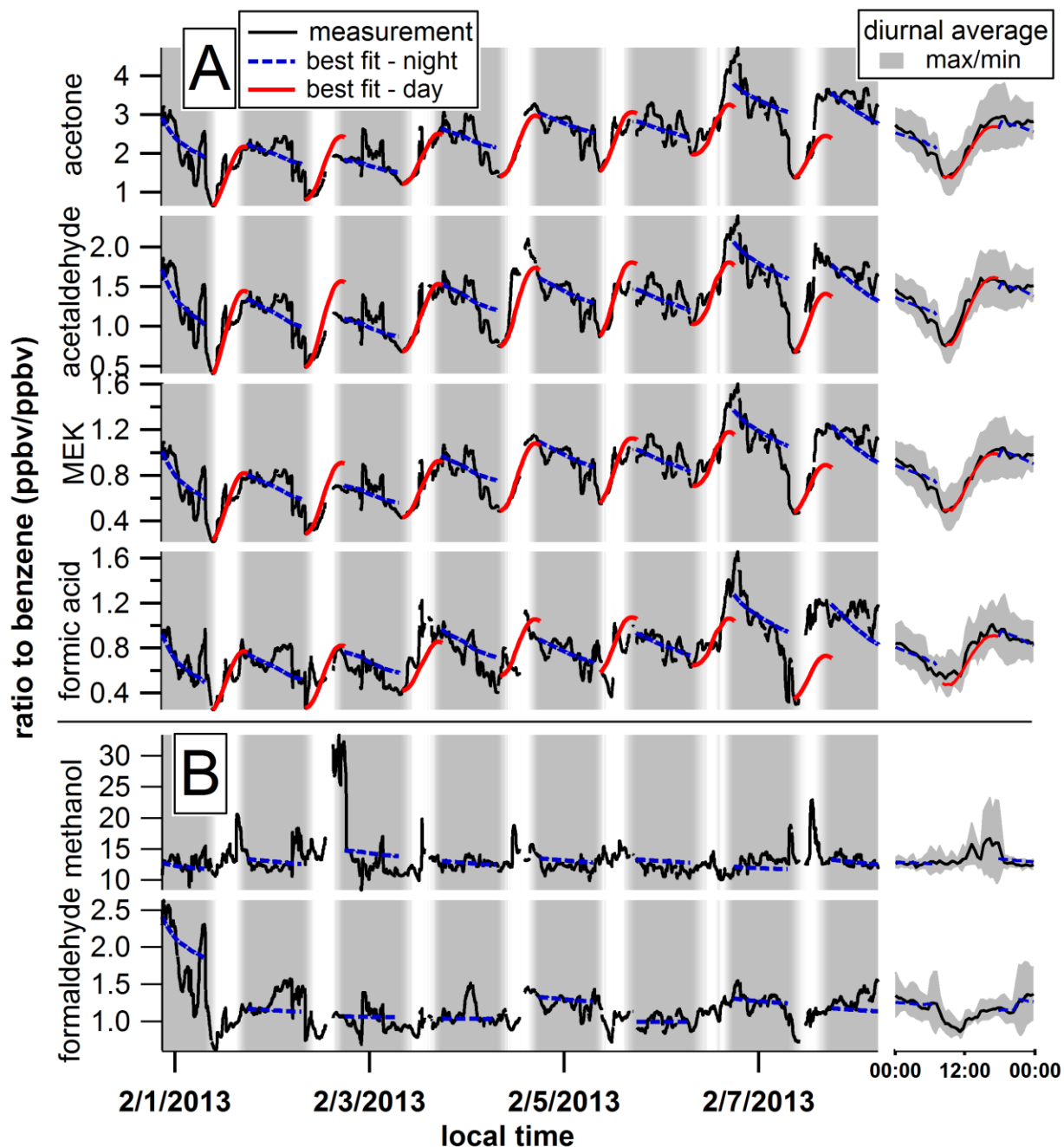
Figure 9. Analysis results for oxygenated compounds. Measured ratio is in black, night best fit in blue, and day best fit in red. A. The best fit is able to reproduce VOC trends during the day for acetone, MEK, acetaldehyde, and formic acid. B. The best fit does not reproduce night time variability or trends in methanol and formaldehyde, which may have substantial primary sources uncorrelated with benzene.
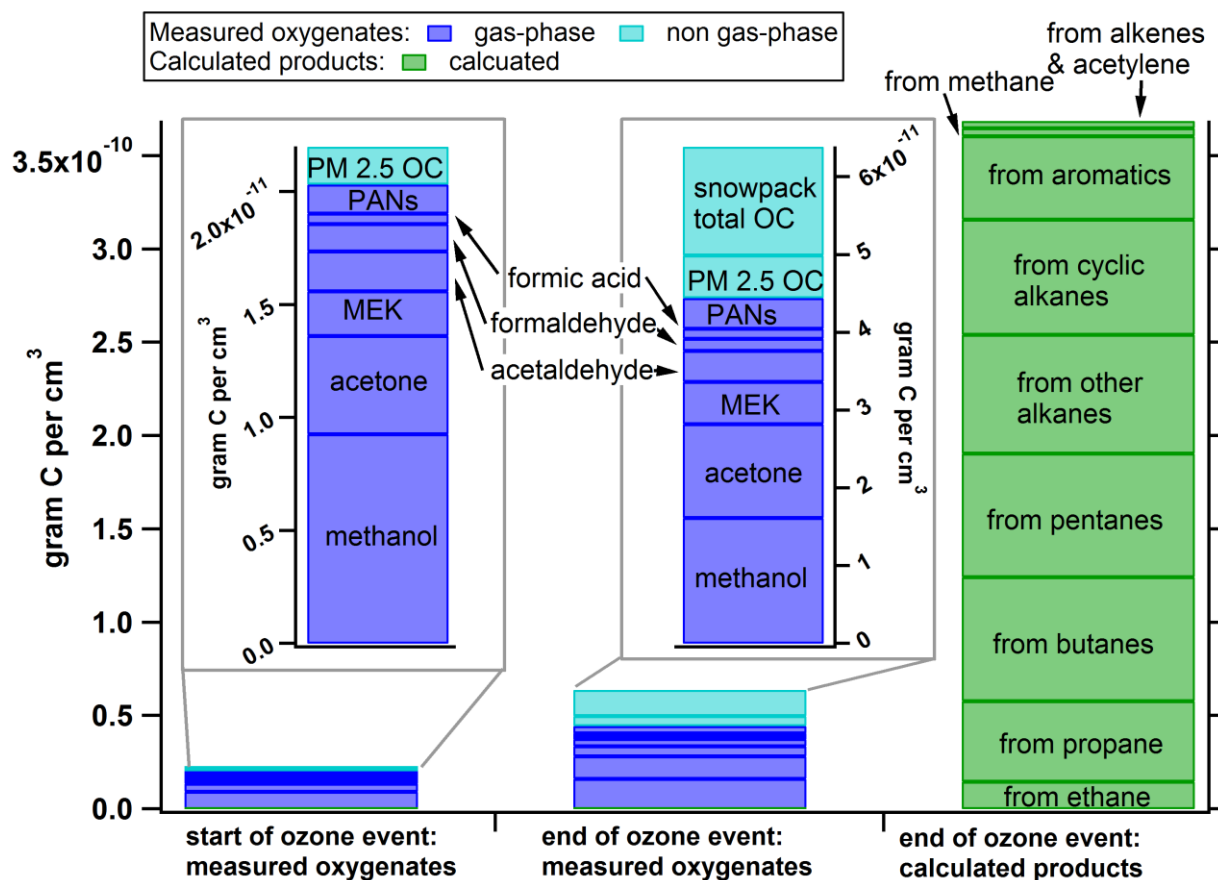
Figure 10. Organic carbon mass of oxygenated and secondary species. The leftmost two bars show the carbon mass of secondary species at the beginning (average of first 12 hours) and end (average of last 12 hours) of the ozone event; speciation is detailed in the two insets. Although methanol and formaldehyde may have primary sources, they are included here in the "product compounds" category to show the maximum contribution of these species to measured products. The rightmost bar shows the calculated mass of secondary compounds at the end of the ozone event; within this bar, the contribution from each precursor is delineated.
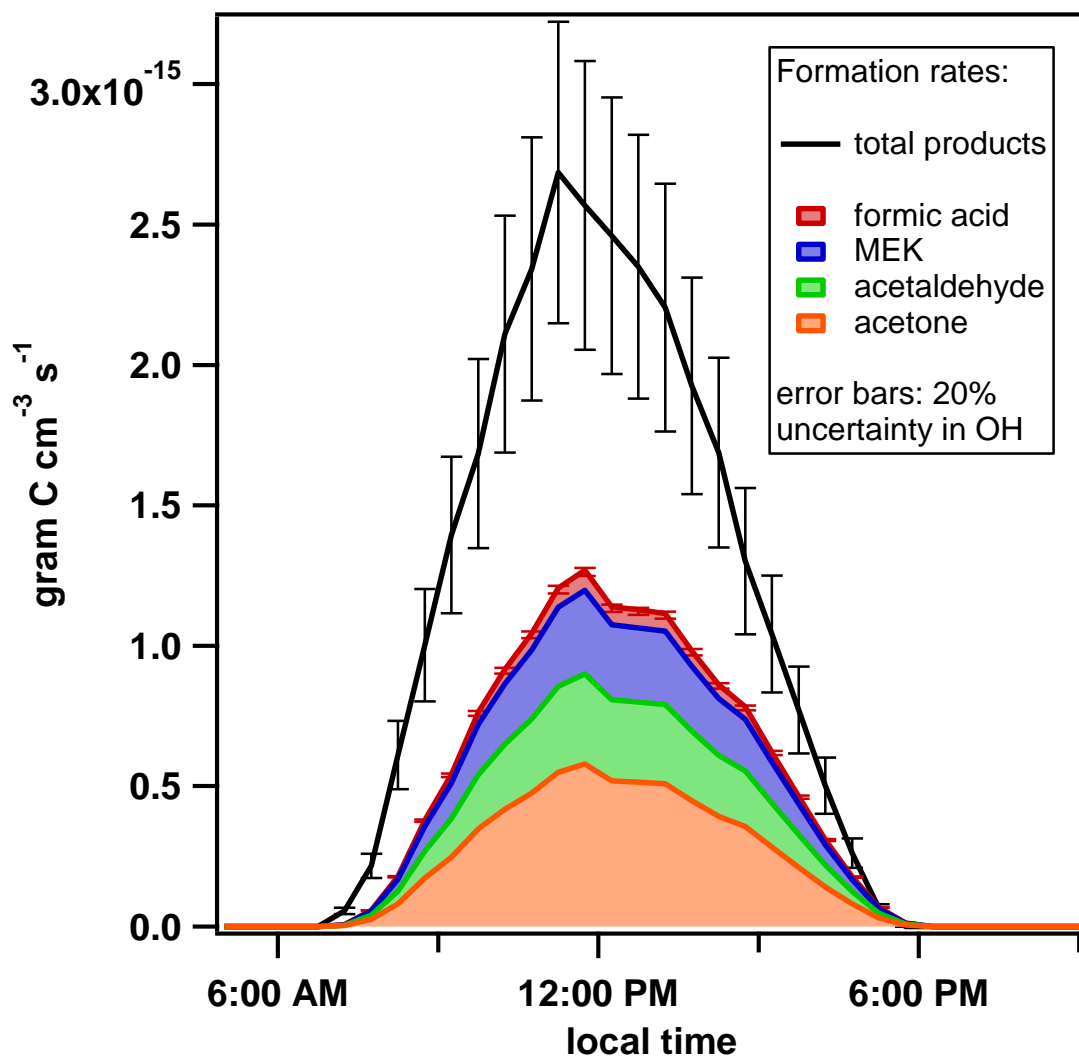
637 Figure 11. Comparison of total product formation rates (black) and measured carbonyl
638 formation rates. There is a substantial gap that indicates the formation of other oxidation
639 products.